2014

Direct chemical synthesis of $L1_0$-FePtAu nanoparticles with high coercivity

Yongsheng Yu
University of Nebraska-Lincoln, Jilin University, yongshengyu80@gmail.com

Pinaki Mukherjee
University of Nebraska-Lincoln, pinaki.mukherjee@rutgers.edu

Yuan Tian
University of Nebraska-Lincoln

Xingzhong Li
University of Nebraska-Lincoln, xli2@unl.edu

David J. Sellmyer
University of Nebraska-Lincoln, dsellmyer@unl.edu

Published in *Nanoscale* 6 (2014), pp. 12050–12055; doi: 10.1039/c4nr02345e

Submitted April 30, 2014; accepted July 17, 2014; published online July 24, 2014.

Supporting information for this article is available following the references.

Direct chemical synthesis of $L1_0$-FePtAu nanoparticles with high coercivity

Yongsheng Yu,[1,2] P. Mukherjee,[1] Yuan Tian,[3] X.-Z. Li,[1] J. E. Shield,[3] and D. J. Sellmyer[1]

1. Nebraska Center for Materials and Nanoscience & Department of Physics and Astronomy, University of Nebraska–Lincoln, Lincoln, NE 68588, USA
2. School of Materials Science and Engineering, Jilin University, Changchun 130025, China
3. Mechanical and Materials Engineering & Nebraska Center for Materials and Nanoscience, University of Nebraska–Lincoln, Lincoln, Nebraska 68588, USA

Corresponding authors – Yongsheng Yu, email yongshengyu80@gmail.com; D. J. Sellmyer, tel. 402-472-2407, fax 402-472-6148, email dsellmyer@unl.edu

Abstract

We report a facile synthesis of hard magnetic $L1_0$-FePtAu nanoparticles by coreduction of $Fe(acac)_3$, $Pt(acac)_2$ (acac = acetylacetonate), and gold acetate in oleylamine. In the current reaction condition, NP sizes are controlled to be 5.5 to 11.0 nm by changing the amount of Au doping. When the Au composition in the NPs is higher than 14%, the hard magnetic NPs are directly obtained without any annealing. The highest coercivity of 12.15 kOe at room temperature could be achieved for the NPs with 32% Au doping, which is much higher than the coercivities reported by the previous studies on solution-synthesized FePt nanoparticles. The reported one-pot synthesis of $L1_0$-FePtAu NPs may help to build superstrong magnets for magnetic or data-storage applications.

Introduction

Hard magnetic nanoparticles (NPs) with a size around 10 nm having a high degree of atomic ordering are needed as building blocks for applications in areas such as magnetic

energy storage, data storage, catalytic chemistry, and biomedicine.[1–10] Recent studies indicate that NdFeB,[11] and hexagonal SmCo[12]-based alloy NPs are ideal building blocks for fabricating nanostructured permanent magnet due to strong ferromagnetism observed within their unique structure. However, rare-earth metal-based alloy NPs of SmCo and NdFeB are extremely difficult to prepare and stabilize due to the easy oxidation of Sm(0) and Nd(0) in the alloy structures. These, plus the limited supply of Sm and Nd, have motivated the search for Sm- and Nd-free alternative magnets.[13] The $L1_0$-intermetallic alloy with face-centered-tetragonal (fct) structure (FePt, CoPt, FePd) with large magnetocrystalline anisotropy constant, high coercivity, and excellent corrosion resistance may be a suitable alternative to the rare-earth permanent magnets.[14–18] The unique properties of the $L1_0$-intermetallic alloy allow reduction of the particles size below 10 nm with simultaneous stabilization of their magnetization against thermal fluctuations and demagnetizing effects.

Recently, solution synthesis has allowed the preparation of monodispersed FePt NPs with a narrow size distribution, compositional control, and well-defined shapes.[19–24] However, the as-synthesized FePt NPs typically adopt a face-centered cubic (fcc) structure, which is unsuitable for data storage and permanent magnetic applications because of the superparamagnetic property of fcc-FePt phase at room temperature. The fcc-to-fct phase transformation requires high temperature (> 550°C) annealing. However, high temperature annealing leads to complete decomposition of the surfactant on the surface of each NP and consequently produces an undesirable aggregation and sintering.[25–28] As a result, the NPs lose their solubility and most importantly their size and shape homogeneity.[29] Therefore, realizing the fcc-to-fct phase transformation without sintering of FePt NPs is one of the major challenges in the production of hard magnetic FePt NPs. To make dispersible $L1_0$-FePt NPs, one can coat the as-synthesized FePt NPs with SiO_2[30] or MgO[31,32] layer before annealing, which serves as a protective layer that prevents FePt sintering during annealing. Then the protective layers can be removed after the fct FePt NPs are formed. Although these methods can reduce sintering and result in hard magnetic FePt NPs at room temperature, high temperature annealing is still required.

Here, we report a new method to directly prepare $L1_0$-FePtAu NPs from solution synthesis. The unique feature of this synthesis is that oleylamine (OAm) in the synthesis serves as surfactant, solvent, and reducing agent at the same time and no other strong reducing agent was used in the synthesis. By simply heating the solution of $Fe(acac)_3$, $Pt(acac)_2$ (acac = acetylacetonate), and gold acetate with OAm to 350°C, $L1_0$-FePtAu NPs can be directly obtained without further annealing. The composition of NPs can be simply controlled by the amounts of $Fe(acac)_3$, $Pt(acac)_2$, and gold acetate used in the synthesis. The work provides a facile general approach to directly synthesize $L1_0$-FePt based NPs may help to build high performance magnets for magnet applications or produce high quality NPs for various catalytic applications.

Materials and methods

Materials

Oleylamine (OAm, > 70%), $Pt(acac)_2$ (acac = acetylacetonate) (99%), and Iron(III) acetylacetonate ($Fe(acac)_3$) (99%) were all purchased from Sigma Aldrich. Gold acetate was purchased from Fisher Scientific. The chemicals and solvents were used as received without purification.

Synthesis of L10-$Fe^{42}Pt^{44}Au^{14}$ NPs

0.25 mmol g of $Fe(acac)_3$, 0.25 mmol of $Pt(acac)_2$, 0.08 mmol of Au acetate, and 10 mL of OAm were first mixed at room temperature. Then the solution was directly heated to 350°C at a heating rate of 5°C min^{-1} and kept at 350°C for 3 h. Then the heating source was removed, and the solution was cooled to room temperature, after which the solution was exposed to air. A black product was precipitated by adding 40 mL of ethanol and separated by centrifugation. Finally, the product was dispersed in hexane.

Characterization

X-ray diffraction (XRD) characterization was carried out on a Rigaku Multiflex diffractometer with Cu $K\alpha$ radiation (λ = 1.5418 Å). The composition analyses of the NPs were carried on FEI Nova Nano SEM450 with energy dispersive spectroscopy (EDS). Samples for transmission electron microscopy (TEM) analysis were prepared by depositing a single drop of diluted particle dispersion in hexane on amorphous carbon-coated copper grids. TEM images, TEM, high-resolution TEM (HRTEM), and the scanning/transmission electron microscopy-EELS (S/TEM-EDS) images were obtained on a FEI Tecnai Osiris with an accelerating voltage of 200 kV. Magnetic properties were measured by a Physical Properties Measurement System (PPMS) up to 70 kOe.

Results and discussion

In the synthesis, we first studied the amount of $Fe(acac)_3$ on the FePt NPs morphology and composition controls. We found that changing the amount of $Fe(acac)_3$ was a simple approach to control FePt NP composition. By changing the amount of $Fe(acac)_3$ from 0.15 mmol to 0.35 mmol and keeping 0.25 mmol of $Pt(acac)_2$, $Fe_{37}Pt_{63}$, and $Fe_{58}Pt_{42}$ NPs could be obtained. Transmission electron microscopy (TEM) analysis showed that the size of the NPs (fig. S1) separated from the amount of $Fe(acac)_3$ were nearly the same. And the morphology of the NPs changed from polyhedral shape to irregular shape. Based on these results, we could synthesize the stoichiometric composition of 49 at.% Fe in FePt NPs by using 0.25 mmol g of $Fe(acac)_3$, 0.25 mmol of $Pt(acac)_2$. Figure 1A shows a typical TEM image of the $Fe_{49}Pt_{51}$ NPs synthesized at 350°C for 3 h with their size being at 5.5 ± 0.5 nm. By controlling the amount of gold acetate (0.08, 0.12, and 0.20 mmol, respectively) added in the reaction, $Fe_{42}Pt_{44}Au_{14}$, $Fe_{38}Pt_{38}Au_{24}$, and $Fe_{34}Pt_{34}Au_{32}$ NPs could be obtained, as shown in figure 1B–D, respectively. It can be clearly seen that the sizes of as-synthesized NPs increase with increasing the composition of Au in the NPs. Doping 14% Au into the NPs yielded 6.5 ± 0.5 nm NPs. By further raising the amount of Au in the NPs from 24% to 32%,

the NP sizes were increased to 9.0 ± 0.8 nm and 11.0 ± 1.0 nm, respectively, indicating that Au additive resulted in a larger particle.

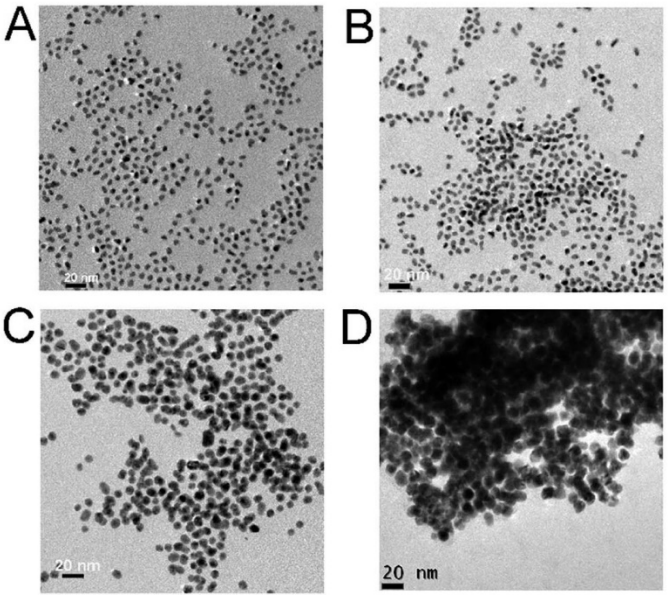

Figure 1. Typical TEM images of (A) $Fe_{49}Pt_{51}$, (B) $Fe^{42}Pt^{44}Au^{14}$, (C) $Fe_{38}Pt_{38}Au_{24}$, and (D) $Fe_{34}Pt_{34}Au_{32}$ NPs.

The crystal structure of the as-synthesized NPs was further characterized by X-ray diffraction (XRD). Figure 2 shows the typical XRD curves of the as-synthesized NPs with different the amount of Au doping. A broad peak ranging from 37° to 44° and a small peak ranging from 44° to 50° are observed for pure $Fe_{49}Pt_{51}$ NPs, which agree with (111) and (200) diffraction peaks, respectively. No other peaks could be observed, which means that the as-synthesized $Fe_{49}Pt_{51}$ NPs have the fcc structure. By doping 14% Au into the NPs, (001) and (110) diffraction peaks appear in the XRD curve. And fcc (200) peak was split into (200) and (002) superlattice diffraction peaks. These results indicate that $L1_0$-FePt phase can be directly obtained from this solution phase synthesis by simply doping with Au element. Further increasing the amount of Au in the NPs, a stronger (001) peak and more splitting between the (200) and (002) peaks can be seen, which means that $L1_0$ phase with higher ordering degree was formed in the as-synthesized NPs. Besides the diffraction peaks from $L1_0$-FePt phase, Au (111), (200), and (311) peaks could be also seen, suggesting that Au phase is also formed during the reaction.

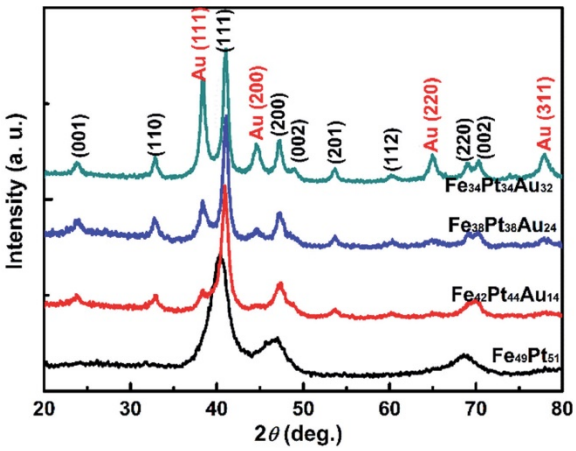

Figure 2. The typical XRD curves of $Fe_{49}Pt_{51}$, $Fe^{42}Pt^{44}Au^{14}$, $Fe_{38}Pt_{38}Au_{24}$, and $Fe_{34}Pt_{34}Au_{32}$ NPs.

Compared with fcc FePt phase, the a lattice constant of fully ordered fct FePt phase expands approximately 2%, while the *c* lattice constant contracts approximately 2.5%, resulting in a *c*/*a* ratio that is less than 1, which means that we can calculate *c*/*a* ratio of the NPs to further characterize whether the NPs are fct structure. Therefore, *c*/*a* ratios versus Au composition in the NPs were calculated from the positions of the (001) and (111) diffraction peaks, as shown in figure 3 (black symbols). For the pure FePt NPs, no (001) peak can be seen, suggesting that the pure FePt NPs are fcc structure and *c*/*a* ratio is equal to 1. After doping 14% Au into FePt NPs, *c*/*a* ratio drops to 0.973, indicating that $Fe_{42}Pt_{44}Au_{14}$ NPs already have the fct structure. With increasing the Au composition in the NPs, *c*/*a* ratios continue to decrease, suggesting that more Au doping could facilitate the formation of fct FePt phase. In order to evaluate the long-range ordering degree of the fct phase for the as-synthesized NPs in more detail, the order parameter *S* is employed. An approximate relation between *S* and *c*/*a* can be written as follows:[33]

$$S^2 = \frac{1-(c/a)}{1-(c/a)_{sf}}$$

where is $(c/a)_{sf}$ the axial ratio for the fully ordered phase, *c*/*a* ratio is for the partially ordered phase. *S* = 1 in this equation corresponds to the fully ordered phase. *S* is zero for a chemically disordered FePt phase. The long-range order parameters *S* for the NPs with different Au composition were calculated from *c*/*a* ratio, as shown in figure 3 (red symbols). In the case of $Fe_{42}Pt_{44}Au_{14}$ NPs, *S* is 0.858, which indicates that FePt phase in $Fe_{42}Pt_{44}Au_{14}$ NPs is partially ordered. *S* values increase with increasing the amount of Au in the NPs, indicating that increasing Au composition promotes the ordering of the FePt phase in the NPs. These results suggest that we could achieve significant ordering FePt phase without significant agglomeration at 350°C synthesis by doping Au into the NPs.

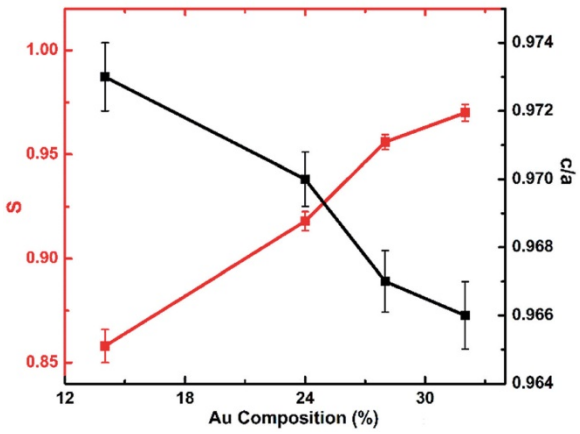

Figure 3. *c/a* ratios and the order parameter *S* versus Au composition in the NPs.

Since there are two phases in the production, it is very important to characterize whether L1$_0$-FePt and Au phases nucleated and grew separately or together. Figure 4A shows the HRTEM image of a representative L10-Fe$_{38}$Pt$_{38}$Au$_{24}$ NP from figure 1C. It can be clearly seen that the NP shows a typical polycrystalline structure. Considering that a small difference of lattice-fringe spacing between the L10-FePt and fcc Au lattice, it is very difficult to clearly distinguish which part is L10-FePt phase and which part is Au phase from HRTEM image. The fast-Fourier transform (FFT) of HRTEM image was used to determine the crystalline structure in the NP, as shown in figure 4B. The FePt (200), Au (111), and Au (200) spots could be indexed in the FFT image, which suggests that L10-FePt and Au phases nucleated together. The angle between Au (111) and Au (200) reflections clearly shows more than one Au lattice within the particle. In order to further confirm that one NP contains L10-FePt and Au two phases, the high-angle annular dark field (HAADF) images of L1$_0$-Fe$_{38}$Pt$_{38}$Au$_{24}$ NPs were also measured, as shown in figure 4C. The corresponding composition distributions in figure 4C were further characterized by the scanning/transmission electron microscopy-EDS (S/TEM-EDS). Figure 4D–H show the elemental mappings of Fe (green), Pt (blue), and Au (red) in each NP. The color distribution within each NP indicates that each NP contains Fe, Pt, Au elements. Combining XRD and HRTEM measurements with elemental mappings, it can be concluded that L1$_0$-FePt and Au phases are segregated in each NP.

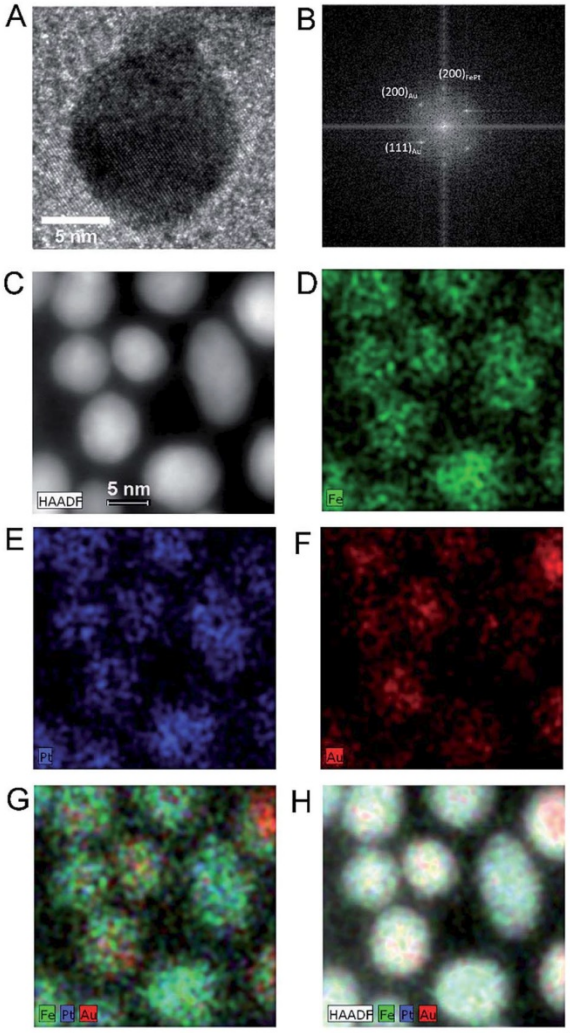

Figure 4. (A) HRTEM image of a representative NP shown in figure 1C. (B) Fast Fourier transform of the HRTEM image. (C) HAADF image of representative $L1_0$-$Fe_{38}Pt_{38}Au_{24}$ NPs. (D–G) Elemental mappings of Fe (green), Pt (blue), and Au (red) signals combined (G) and single element Fe (green) (D), Pt (blue) (E), and Au (red) (F). (H) HAADF image and the corresponding elemental map of representative $L1_0$-$Fe_{38}Pt_{38}Au_{24}$ NPs.

The magnetic properties of the as-synthesized NPs were measured using a Quantum Design Physical Property Measurement System (PPMS). Figure 5 shows the hysteresis loops of the as-synthesized NPs with different the amount of Au doping measured at room temperature. For the pure FePt NPs, the NPs possess soft magnetic properties with a coercivity of 0.09 kOe. When the NPs were doped by 7% Au, the coercivity of the NPs increases to 0.26 kOe. The corresponding hysteresis loop shows two-phase behavior, which means that the partially ordered FePt phase started to form in the NPs by doping a small amount of Au. A coercivity of 4.50 kOe could be achieved when Au composition in the NPs reaches

14%, indicating that the NPs contain hard magnetic FePt phase. Increasing the Au additive to the NPs results in the higher coercivity of the samples. When the Au additives are 24% and 28%, the coercivities of the NPs increase to 9.58 and 10.85 kOe, respectively. Further increasing the Au composition to 32% in the NPs, the coercivity of 12.15 kOe could be obtained, which is much higher than the coercivities reported by the previous studies on solution-synthesized FePt NPs. The M_s values first increase with increasing the Au composition to 14%. The reason for this might be related to the reduced magnetization on the surfaces of the smaller NPs. Further increasing the Au composition led to a decrease in saturation magnetization of the NPs, due to large amount of nonmagnetic Au in the NPs.

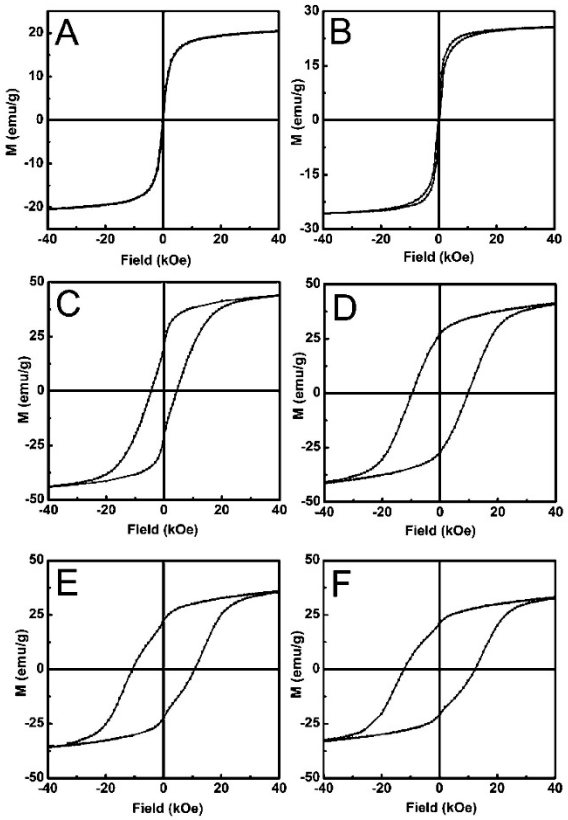

Figure 5. The hysteresis loops of the as-synthesized NPs: (A) $Fe_{49}Pt_{51}$, (B)$Fe_{46.5}Pt_{46.5}Au_7$, (C) $Fe_{42}Pt_{44}Au_{14}$, (D) $Fe_{38}Pt_{38}Au_{24}$, (E) $Fe_{31}Pt_{31}Au_{28}$ and (F) $Fe_{34}Pt_{34}Au_{32}$ NPs.

To understand the formation mechanism of $L1_0$-FePt phase in the NPs, the synthesis temperature was changed from 230 to 390°C and 0.25 mmol g of $Fe(acac)_3$, 0.25 mmol of $Pt(acac)_2$, 0.12 mmol of gold acetate were used in the reaction. For 230, 260, and 290°C synthesis for 3 h, $Fe_{43}Pt_{43}Au_{14}$, $Fe_{41.5}Pt_{41.5}Au_{17}$ and $Fe_{40}Pt_{40}Au_{20}$ NPs could be obtained, as shown in figure S2. These results suggest that Au composition in the NPs increase with increasing the synthesis temperature. Figure 6 shows the XRD curves of the NPs synthesized at different temperature, indicating the evolution of the $L1_0$ phase with increasing synthesis

temperature. For 230°C synthesis, only fcc FePt (111) and (200) peaks can be seen. No Au peaks appear in the XRD curve, which means that Au atoms entered into the fcc FePt lattice. With increasing the synthesis temperature to 260°C, Au (111) peak appeared at the left side of fcc FePt (111) peak, suggesting that Au atoms segregated from fcc FePt lattice. When the synthesis temperature was increased to 290°C, $L1_0$-FePt (001), (110), and (002) peaks can be observed and Au (111) and $L1_0$-FePt (111) peaks were completely divided, which means that ordered FePt phase was formed. Figure S3 shows the hysteresis loops of the NPs synthesized at different temperature. We can clearly see that the NPs synthesized at 230°C show the typical softmagnetic properties. Increasing the synthesis temperature to 260°C, the coercivity of the NPs is about 0.90 kOe, which means that the FePt phase in the NPs started to order. Further increasing the synthesis temperature to 290°C, the NPs have 5.53 kOe coercivity. These results suggest that the phase separation between Au and FePt promotes the ordering of the FePt phase in the NPs. From these results, we can see that at low temperature synthesis, Fe, Pt, and Au atoms nucleated together and alloy FePtAu NPs with fcc structure can be formed. With an increase of the synthesis temperature, Au atoms would diffuse out of the fcc FePt lattice, creating lattice vacancies that increase the mobility of Fe and Pt atoms to rearrange to fct phase.

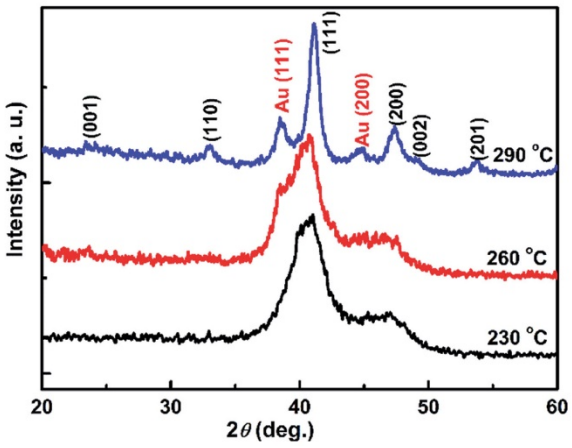

Figure 6. The XRD curves of the NPs synthesized at different temperature.

Conclusions

We have developed a facile one-pot synthesis of $L1_0$-FePtAu NPs through a high-temperature solution synthesis by using $Fe(acac)_3$, $Pt(acac)_2$, and gold acetate as precursors in the presence of OAm. The unique feature of this synthesis is that OAm in the synthesis serves as surfactant, solvent, and reducing agent at the same time. Through controlling Au composition in the NPs, we can obtain NPs with sizes from 5.5 to 11.0 nm. When the Au composition in the NPs is higher than 14%, the hard magnetic NPs can be directly obtained without any annealing. The highest coercivity of 12.15 kOe can be achieved for the NPs with 32% Au doping, which is much higher than the coercivities reported by the previous

studies on solution-synthesized FePt NPs. The phase separation between Au and FePt phase likely is the main reason for the ordering of FePt phase. The reported one-pot synthesis of $L1_0$-FePtAu NPs may provide an ideal class of building blocks for magnetic energy and data-storage applications.

Acknowledgments – This work was supported by the National Natural Science Foundation of China under Grant (no. 51101069), the US Department of Energy (Grant no. DE-FG02–04ER46152, magnetic characterization), the US Army Research Office (W911NF-10-2-0099, structural characterization), and NSF (NSFDMR-0960110, major research instrumentation). The research was performed in part in central facilities of the Nebraska Center for Materials and Nanoscience (which is supported by the Nebraska Research Facilities).

Notes and references

1. S. H. Sun, C. B. Murray, D. Weller, L. Folks, and A. Moser, *Science*, 2000, 287, 1989–1992.
2. D. J. Sellmyer, *Nature*, 2002, 420, 374–375.
3. S. J. Guo, S. Zhang, and S. H. Sun, *Angew. Chem., Int. Ed.*, 2013, 52, 8526–8544.
4. C. Wang, M. Chi, D. Li, D. van der Vliet, G. Wang, Q. Lin, J. F. Mitchell, K. L. More, N. M. Markovic, and V. R. Stamenkovic, *ACS Catal.*, 2011, 1, 1355–1359.
5. Y. Kang, J. B. Pyo, X. Ye, T. R. Gordon, and B. C. Murray, *ACS Nano*, 2012, 6, 5642–5647.
6. J. Kim, Y. Lee, and S. H. Sun, *J. Am. Chem. Soc.*, 2010, 132, 4996–4997.
7. C. J. Xu, Z. L. Yuan, N. Kohler, J. Kim, M. A. Chung, and S. H. Sun, *J. Am. Chem. Soc.*, 2009, 131, 15346–15351.
8. B. Balamurugan, B. Das, V. R. Shah, R. Skomski, X. Z. Li, and D. J. Sellmyer, *Appl. Phys. Lett.*, 2012, 101, 122407–122409.
9. S. Zhang, S. J. Guo, H. Y. Zhu, D. Su, and S. H. Sun, *J. Am. Chem. Soc.*, 2012, 134, 5060–5063.
10. Z. Jia, S. Kang, D. E. Nikles, and J. W. Harrell, *IEEE Trans. Magn.*, 2005, 41, 3385–3387.
11. W. B. Cui, Y. K. Takahashi, and K. Hono, *Adv. Mater.*, 2012, 24, 6530–6535.
12. Y. L. Hou, Z. C. Xu, S. Peng, C. B. Rong, J. P. Liu, and S. H. Sun, *Adv. Mater.*, 2007, 19, 3349–3352.
13. M. J. Kramer, R. W. McCallum, I. A. Anderson, and S. Constantinides, *J. Miner. Met. Mater. Soc.*, 2012, 64, 752–763.
14. Y. S. Yu, K. W. Sun, Y. Tian, X.-Z. Li, M. J. Kramer, D. J. Sellmyer, J. E. Shield, and S. H. Sun, *Nano Lett.*, 2013, 13, 4975–4979.
15. H. Zeng, J. Li, J. P. Liu, Z. L. Wang, and S. H. Sun, *Nature*, 2002, 420, 395–398.
16. H. Zeng, J. Li, Z. L. Wang, J. P. Liu, and S. H. Sun, *Nano Lett.*, 2004, 4, 187–190.
17. S. H. Sun, *Adv. Mater.*, 2006, 18, 393–403.
18. H. Zeng, M. L. Yan, N. Powers, and D. J. Sellmyer, *Appl. Phys. Lett.*, 2002, 80, 2350–2352.
19. A. Figuerola, A. Fiore, R. D. Corato, A. Falqui, C. Giannini, E. Micotti, A. Lascialfari, M. Corti, R. Cingolani, T. Pellegrino, et al., *J. Am. Chem. Soc.*, 2008, 130, 1477–1487.
20. V. Nandwana, K. E. Elkins, N. Poudyal, G. S. Chaubey, K. Yano, and J. P. Liu, *J. Phys. Chem. C*, 2007, 111, 4185–4189.
21. M. Chen, J. P. Liu, and S. H. Sun, *J. Am. Chem. Soc.*, 2004, 126, 8394–8395.
22. S. H. Sun, E. E. Fullerton, D. Weller, and C. B. Murray, *IEEE Trans. Magn.*, 2001, 37, 1239–1243.
23. X. W. Teng and H. Yang, *J. Am. Chem. Soc.*, 2003, 125, 14559–14563.

24. N. Poudyal, G. S. Chaubey, C. Rong, and J. P. Liu, *J. Appl. Phys.*, 2009, 105, 07A749–07A751.
25. L. C. Varanda and M. Jafelicci, *J. Am. Chem. Soc.*, 2006, 128, 11062–11066.
26. M. Chen, T. Pica, Y. B. Jiang, P. Li, K. Yano, J. P. Liu, A. K. Datye, and H. Fan, *J. Am. Chem. Soc.*, 2007, 129, 6348–6349.
27. C. Wang, Y. L. Hou, J. Kim, and S. H. Sun, *Angew. Chem., Int. Ed.*, 2007, 46, 6333–6335.
28. M. Chen and D. E. Nikles, *Nano Lett.*, 2002, 2, 211–214.
29. I. Zafiropoulou, E. Devlin, N. Boukos, D. Niarchos, D. Petridis, and V. Tzitzios, *Chem. Mater.*, 2007, 19, 1898–1900.
30. Y. Tamada, S. Yamamoto, M. Takano, S. Nasu, and T. Ono, *Appl. Phys. Lett.*, 2007, 90, 162509–162511.
31. J. Kim, C. B. Rong, J. P. Liu, and S. H. Sun, *Adv. Mater.*, 2009, 21, 906–909.
32. J. Kim, C. B. Rong, Y. Lee, J. P. Liu, and S. H. Sun, *Chem. Mater.*, 2008, 20, 7242–7245.
33. B. W. Roberts, *Acta Metall.*, 1954, 2, 597–603.

Supplementary Information

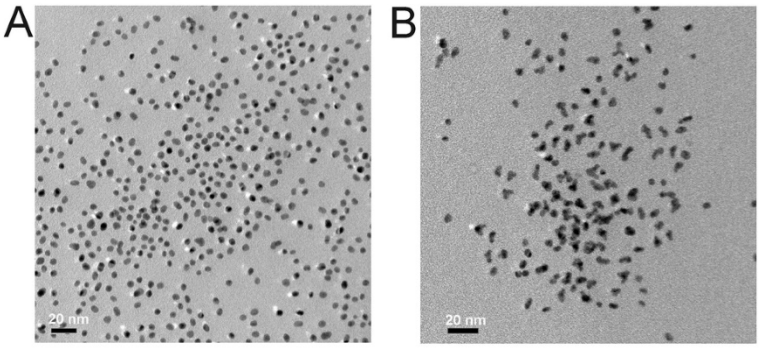

Figure S1. TEM images of (A) $Fe_{37}Pt_{63}$ and (B) $Fe_{58}Pt_{42}$ NPs.

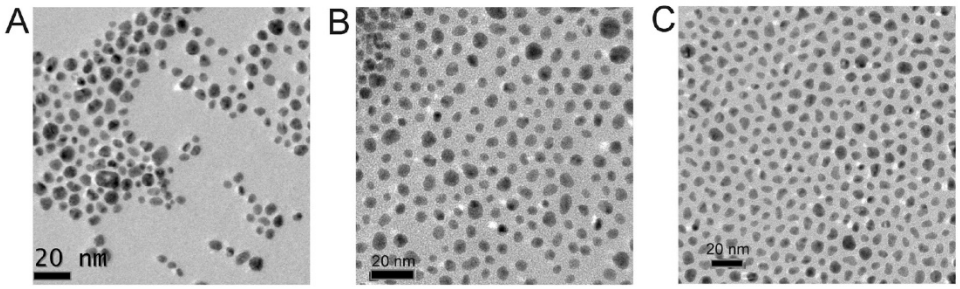

Figure S2. TEM images of (A) $Fe_{43}Pt_{43}Au_{14}$, (B) $Fe_{41.5}Pt_{41.5}Au_{17}$ and (C) $Fe_{40}Pt_{40}Au_{20}$ NPs.

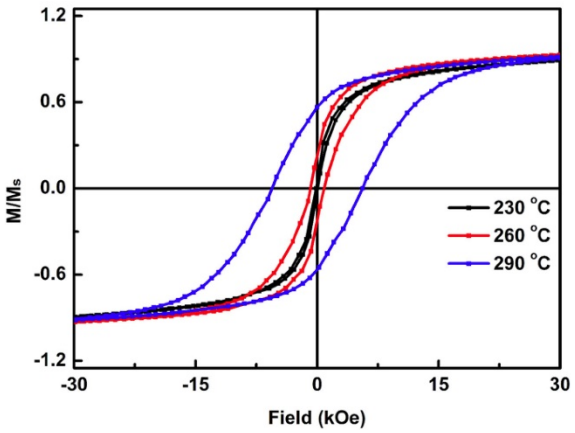

Figure S3. Hysteresis loops of the NPs synthesized at different temperatures.